Geophysical Research Letters

RESEARCH LETTER
10.1029/2021GL092719

Key Points:

- Increased ocean resolution affects North Atlantic winter climate by modifying the location of Gulf Stream
- Future projection of eddy-rich model shows a decrease in the Gulf Stream separation from the coast and a stronger warming hole
- Eddy-rich model projects a more pronounced change in east Atlantic storminess and precipitation than eddy-permitting model

Supporting Information:

Supporting Information may be found in the online version of this article.

Correspondence to:

J. P. Grist,
jeremy.grist@noc.ac.uk

Citation:

Grist, J. P., Josey, S. A., Sinha, B., Catto, J. L., Roberts, M. J., & Coward, A. C. (2021). Future evolution of an eddy rich ocean associated with enhanced east Atlantic storminess in a coupled model projection. *Geophysical Research Letters*, *48*, e2021GL092719. https://doi.org/10.1029/2021GL092719

Received 27 JAN 2021
Accepted 8 MAR 2021

Future Evolution of an Eddy Rich Ocean Associated with Enhanced East Atlantic Storminess in a Coupled Model Projection

Jeremy P. Grist[1], Simon A. Josey[1], Bablu Sinha[1], Jennifer L. Catto[2], Malcolm J. Roberts[3], and Andrew C. Coward[1]

[1]National Oceanography Centre, Southampton, UK, [2]College of Engineering, Mathematics and Physical Sciences, University of Exeter, Exeter, UK, [3]Met Office, Exeter, UK

Abstract Improved representation of air-sea fluxes afforded by eddy-rich oceans in high-resolution coupled ocean-atmosphere models may modify the tracks and intensity of storms and their response to climate change. We examine changes in winter surface ocean conditions and storminess associated with moving from an eddy-permitting (1/4°, HM) to an eddy-rich (1/12°, HH) ocean in control and climate change (SSP585) simulations of the HadGEM3-GC3.1 model in which atmosphere resolution is kept at 25 km. Differences in North Atlantic climate in the control runs stem from a revised location of the Gulf Stream in the eddy-rich model. Projections reveal greater warming in the western Atlantic in HH than HM and a pronounced increase in eastern Atlantic storminess with changes six times greater than in the eddy-permitting model. This increase is associated with the distinctive long-term evolution of the North Atlantic warming hole and the Gulf Stream separation in the eddy-rich model.

1. Introduction

Although the highest resolution ocean for most climate models contributing to CMIP6 (The Coupled Model Intercomparison Project Phase 6) is of the order ¼°, i.e., eddy-permitting, there are now a few contributing models with near eddy-resolving or eddy-rich (~1/12°) oceans (Chang et al., 2020). This paper considers if, in one such model, the move to eddy-rich ocean resolution is associated with changes in the depiction of mid-latitude North Atlantic storms and their sensitivity to anthropogenic climate change.

The IPCC Fifth Assessment Report (AR5) concluded that there is low confidence in future projections of Northern Hemisphere winter storm tracks (Collins et al., 2013). Multi-model means displayed an increase in precipitation over the North Atlantic storm track as well as a modest increase in storminess in a south-west to north-east band in the eastern Atlantic over the British Isles, but a reduction to the north and south of this band (Zappa et al., 2013). The different prominence that simulations place on processes that decrease storm baroclinic growth rate such as polar amplification versus those that increase it, such as an increase in mid-latitude sea-surface temperature (SST) gradient from a decline in the Atlantic Meridional Overturning Circulation (AMOC, Woolings et al., 2012), could be a factor in the relatively small change seen in the ensemble mean of the models.

A constraint on previous studies of CMIP5 models has been their biases in the depiction of mid-latitude storms. In this regard, a recent analysis has found CMIP6 models significantly reduce biases in storm track latitude, tilt, and in the frequency of the most intense cyclones (Priestley et al., 2020). Much of the improvement in the Northern Hemisphere was attributed to increased atmospheric resolution. This is consistent with a comparison of the response of synoptic fronts to an SST front in 1° and 0.25° resolution atmosphere-only models (Smirnov et al., 2015). In the higher resolution atmosphere simulation the vertical circulation and the horizontal heat transport were more extensive and stronger respectively and in closer agreement with observations.

While greater fidelity in present-day and projected simulations does not necessarily follow from the higher atmosphere or ocean resolution alone (Collins et al., 2018), previous work implies that the move to an eddy-rich ocean could have a significant impact on North Atlantic mid-latitude storms. Evidence for the importance of ocean resolution comes from a study of a numerical weather prediction model forced with

eddy-rich and non-eddy rich SST fields (Ma et al., 2015). The move to an eddy-rich SST field affected surface sensible and latent heat fluxes over the Kuroshio Extension as the increase in atmospheric heat gain from warm eddies is greater than the reduction in gain from cold eddies. More recently, Siqueira et al. (2021) suggest, based on observational estimates and eddy-resolving coupled retrospective forecasts, that Kuroshio Extension variability affects rainfall along the west coast of North America; in contrast, their eddy-parameterized model showed no sensitivity to Kuroshio Extension variability. Other atmospheric-only model-based studies have shown how eddy-scale SST features, including the GS representation, affect the growth rate, vertical motion, and precipitation of extratropical cyclones (Czaja et al., 2019; Giordani & Caniaux, 2001; Sheldon et al., 2017). For example, with the framework of atmospheric reanalysis, it has been demonstrated that a high-resolution ocean is necessary to adequately simulate the strong cross GS gradients in SST and surface turbulent fluxes that enhance precipitation from transient frontal systems (Parfitt et al., 2017). Similarly, Vanniere et al. (2017) forced a regional mesoscale atmosphere model with observed and smoothed SSTs. They found that with a stronger SST gradient there was greater circulation across, and more convective rainfall along the GS. They emphasize that the convection was directly forced by the SST as opposed to the SST gradient, but that the sharp difference in convection across the front helped drive the cross SST front circulation.

Eddy-rich oceans have also been shown to lead to a stronger and less meandering Kuroshio Extension (Ma et al., 2016), a result which likely has similar implications for the GS. In ocean-only models, Marzocchi et al. (2015) showed that the poor simulation of the separation of the GS from the US coast often found in 1/4° ocean models was greatly improved between ¼° and 1/12° versions of the same ocean model. Although there is some agreement that a higher (eddy-rich) ocean resolution appears to be a necessary component to achieve accurate GS separation, on its own, it is not sufficient, and thus it remains an important area of investigation (Chassignet & Marshall, 2008; Schoonover et al., 2017; Zhang & Vallis, 2007). For example, using a regional coupled model, Renault et al. (2016) argue the air-sea momentum coupling that allows GS ocean currents to modulate the surface stress and the eddy activity is important for reducing the bias in the GS separation.

If the improved GS simulation noted by Marzocchi et al. (2015) in ocean-only models is found in global coupled models, similar improvements in air-sea heat fluxes and surface temperature gradients may also be expected. The improved representation of surface fluxes and temperature gradients could allow some mechanisms to improve the simulation of mid-latitude storms and their future projections. For example, near-surface horizontal temperature gradients in the vicinity of the GS are important for storm growth (de Vries et al., 2019). If sufficiently strong, cross GS gradients in heat flux can be strengthened by the passage of cold fronts (Parfitt et al., 2016), the major source of precipitation in oceanic storm tracks (Catto et al., 2012). In addition, the location of the warmest GS waters will strongly affect the maximum air-sea temperature difference in the region (Small et al., 2019), with the corresponding changes in latent and sensible heat flux influencing storm growth (Booth et al., 2012; Kuo et al., 1991). Furthermore, more intense heat loss and convection over warm ocean eddies themselves could further influence storm development (Foussard et al., 2019).

A previous comparison between non-eddy resolving and eddy-rich versions of two climate models found that the resolution-induced changes in the SST gradient had little effect on the storm track, although the absolute change in SST was important (Small et al., 2019). In particular, in the Community Earth System Model version 1 (CESM1), an eddy-rich simulation reduced the warm SST bias adjacent to the United States coast, reducing the storm track strength near the GS by 20% and improving the location of the nearby storm track maximum. The present study differs from Small et al. (2019) in that we examine the difference between ¼° and 1/12° ocean resolution (as opposed to ~1° and ~1/10°). This is the resolution change when there is typically a step-change in GS simulation (Bryan et al., 2007; Marzocchi et al., 2015). This study is also concerned with how the resolution impacts future projections of the mid-latitude surface storm track's location and strength.

The structure of the manuscript is as follows. In Section 2, the model and the simulations used are described. In Section 3, the results of the comparison between eddy-permitting and eddy-rich models are presented. The conclusions are summarized in Section 4.

2. Model, Simulations, Analysis

The model used is the Hadley Center Global Environment Model 3—Global Coupled vn 3.1 (HadGEM3-GC3.1) (Williams et al., 2017). Two resolutions are compared; HM, which has a 25 km atmosphere and an eddy-permitting (~25 km, ¼°) ocean, and HH, which has the same resolution atmosphere and an eddy-rich (~8 km, 1/12°) ocean, with the same 75 levels in the vertical (Roberts et al., 2019). First, to establish the most robust resolution-dependent differences between HH and HM, we compare their "control-1950" simulations (Coward & Roberts, 2018). These are 100-years simulations run with constant radiative forcing of the 10-years 1950s climatology (Haarsma et al., 2016). Second, we establish the climate change signal in both HH and HM and examine how they differ. This is done by examining the same 1950–2050 climate change projection for both HH and HM. The projection has two parts, 1950–2014 is the historical forcing simulation (hist-1950, Roberts et al., 2017a) and 2015–2050 is a future projection (highres-future, Roberts et al., 2017b) which has time-varying external forcings following the SSP585 future scenario (Riahi et al., 2017). Designed to represent emissions high enough to produce a radiative forcing of 8.5 W m^{-2} in 2100, SSP585 is the most similar CMIP6 scenario to the RCP8.5 in CMIP5. The spin-up protocols are described in Roberts et al. (2019). To establish the climate change signal for both resolutions, we compare the first 20 years of the historical 1950–2014 forcing simulation (hist-1950) (Roberts et al., 2017a) with the last 20 years of the 2015–2050 future projected forcing (highres-future) and examine century-long trends in the relevant 1950–2050 climate change projections.

The analysis focuses on December, January, and February (DJF) for the North Atlantic region. As measures of storm track intensity, we use the standard deviation of the daily difference in the surface meridional wind (Booth et al., 2017) (hereafter the surface storm track) and mean DJF precipitation as used by Small et al. (2019). Surface storm tracks have a different climatological pattern to other indices at, for example, 850 hPa, and are a particularly useful measure in regions such as the Gulf Stream where the ocean has a greater role (Booth et al., 2017). The statistical significance of the difference of the winter means is calculated using the *t*-test for large samples (control runs differences) and a look-up table test for small samples (for 2031–2050 minus 1951–1970) following Zwiers and Von Storch (1995). Model simulations are compared to 40 years of ERA5 reanalysis (1979–1980 to 2018–2019, Hersbach et al., 2020).

3. Results

3.1. Differences in the Control Simulations

We display the difference between HH and HM control runs for DJF in Figure 1: (a) SST, (b) lower tropospheric (925 hPa) temperature gradient, (c) sensible heat flux, (d) latent heat flux, (e) total precipitation, (f) convective precipitation, and (g) storm track intensity. In terms of SST, the key difference between HH and HM is that HH is predominantly warmer in the north Atlantic (though not globally, Figure S1). The other major SST difference is that in HH the temperature is lower in the GS extension region. This is indicative of the HH GS separating from the North American coast at Cape Hatteras, unlike in HM where it stays adjacent to the coast until ~39ºN. The difference in GS location will be discussed further later, but for now we note that it is the most significant change in the SST field globally (see also Roberts et al., 2019, Figure 7k) and it leaves an imprint on the subsequent fields relevant to North Atlantic winter storms. Specifically, the SST shift is accompanied by a similar shift in the 925 hPa temperature gradient, which in HH is weaker adjacent to the US coast between 30 and 40ºN but stronger to the south-east by up to 10^{-5}ºC m^{-1} (i.e., an extra 1 °C in 100 km).

The cooler coastward and warmer oceanward SSTs in the region of the GS in Figure 1a) are also accompanied by significant respective decreases and increases in both sensible and latent heat flux from the ocean to the atmosphere (Figures 1c and 1d). Interest in these fields stems from the near surface temperature gradient being important for storm growth (e.g., de Vries et al., 2019; Nakamura et al., 2004) and strong surface fluxes promoting an unstable air-sea interface (Small et al., 2019). To first order, the HH SST increases (decreases) are co-located with significant increases (decreases) in precipitation, such that increased precipitation is found south of the GS (65ºW to 35ºW and 30ºN to 40ºN) and additionally further north (near 35ºW and 50ºN) and east (20ºW and 55ºN) along the Atlantic storm track (Figure 1e). The strong contribution of convective precipitation (Figure 1f) to the changes supports the contention (Booth et al., 2017;

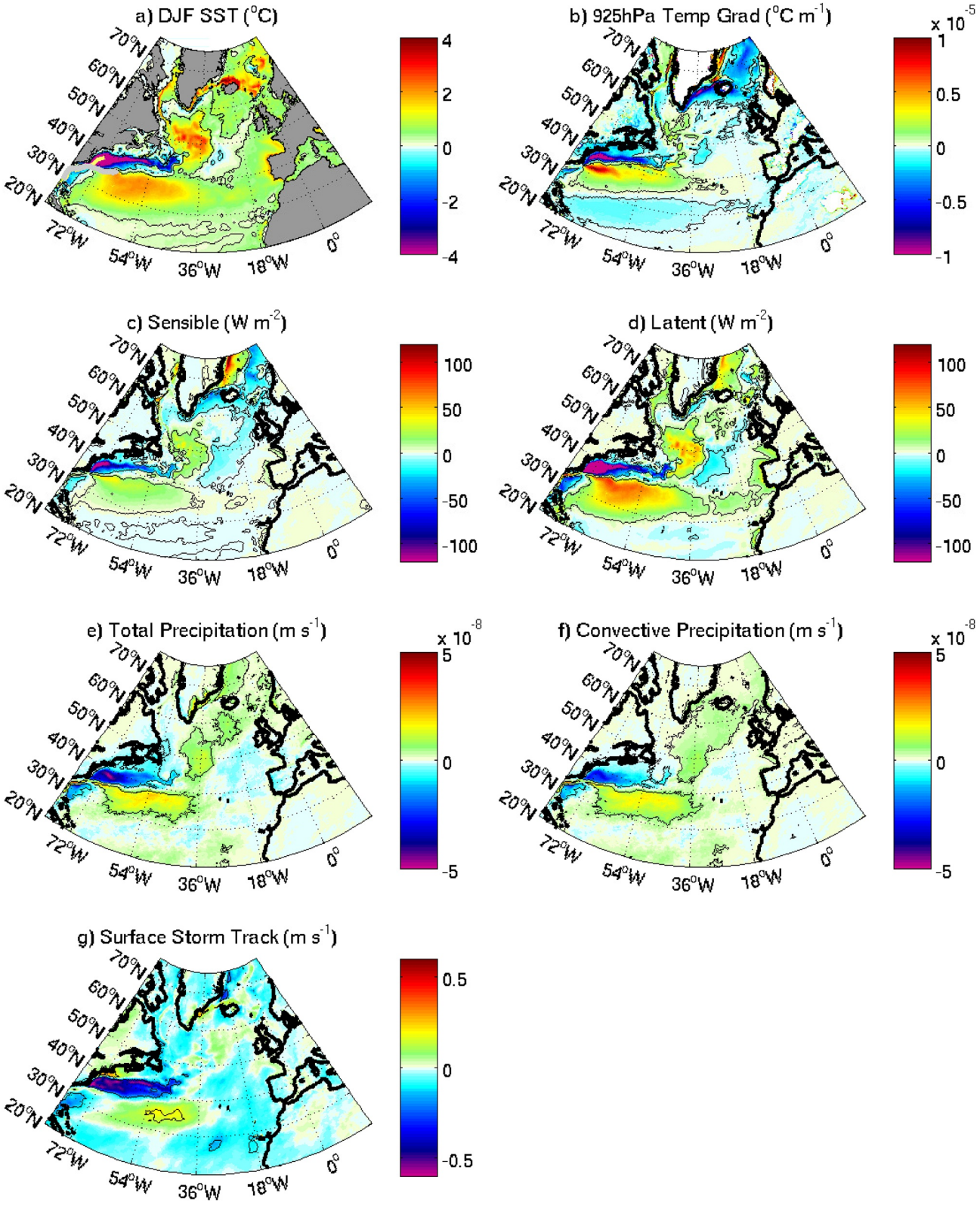
a) DJF SST (°C)
b) 925hPa Temp Grad (°C m-1)
c) Sensible (W m-2)
d) Latent (W m-2)
e) Total Precipitation (m s-1)
f) Convective Precipitation (m s-1)
g) Surface Storm Track (m s-1)
70°N
60°N
50°N
40°N
30°N
20°N
72°W
54°W
36°W
18°W
0°
x 10-5
x 10-8

Small et al., 2019) that the precipitation changes are directly driven by the SST changes associated with the eddy-rich ocean in HH. In terms of changes to storminess (Figure 1g), unlike the precipitation these are largely confined to the western Atlantic GS region, with a significant decrease of −0.6 m s^{-1} over the GS, and an increase of up to 0.2 m s^{-1} to the south-east. These changes could be related to changes in SST or temperature gradient—as the spatial pattern is similar to both.

Summarizing Figure 1, the move to the eddy-rich ocean results in significant differences in the Atlantic surface storm track and related fields. These differences ultimately stem from either one of, or a combination of the two significant differences in SST, namely a predominantly warmer North Atlantic and a revised location of the GS in the eddy-rich ocean climate model. We note the nature of the global simulations does not eliminate the possibility that resolution change leads to changes in another ocean basin which in turn exert a remote influence on Atlantic storms. However, we note that the SST changes in other basins are minor compared to the North Atlantic and the GS in particular (see Figure S1). We also note that similar basin wide changes associated with the GS shifts have previously been found in both observed air-sea fluxes (Joyce et al., 2009; Parfitt & Kwon, 2020, relative to the overlying jet) and atmosphere only model experiments of mid-latitude Atlantic storms (Lee et al., 2018).

3.2. Comparisons With Observations in the Gulf Stream Region

Since the largest changes in precipitation and storm tracks have been identified as being associated with the GS, this change is examined in more detail and with reference to ERA5 observations (ERA5 SST is a combination of the UKMet. Office HadISST2 and OSTIA products, Hirahara et al., 2016). The mean DJF SST for HM, ERA5 observations and HH are shown in Figures 2a–2c, respectively. It can be seen that in ERA5, the GS front separates from the North American coast at Cape Hatteras (36ºN) to a north-eastward direction. In contrast, in the eddy-permitting model, HM, the GS stays adjacent to the coast until about 38–39ºN, and afterward takes a near zonal track. In the eddy-rich model, HH does (correctly) separate at Cape Hatteras, but it appears to over-correct, as it moves eastward more rapidly than observed. These differences are summarized in Figure 2d, which shows the mean SST across 37ºN latitude.

Interestingly, although the GS location and temperature maximum in HM are closer to ERA5 than HH, this is not the case for the magnitude of the air–sea temperature difference (Figure 2e) or the turbulent air-sea fluxes that it drives (Figure 2f). Because the surface air temperature decreases with proximity to the coast, due to the influence of cold continental air, the smaller bias in HM GS location translates into a 50% greater bias in the maximum air-sea temperature difference. The HM maximum is 2.1°C greater than ERA5 and the HH maximum is 1.4°C less. The HM peak turbulent heat flux also has a much greater bias (106 W m^{-2} greater) relative to ERA5 than HH (which is 39 W m^{-2} less). By comparing Figure 2e with Figure 2f, it is clear to a large extent the resolution changes in latent and sensible heat flux are a consequence of the difference in the air-sea temperature gradient brought about by the change in location of the GS. Specifically on this point, we have included (dashed thin green line) an estimate of the HM sensible flux by scaling the HH sensible heat flux by the ratio of HM:HH air-sea temperature differences. This clearly demonstrates the vast majority of the resolution-dependent difference in air-sea sensible heat flux is explained by the change in air-sea temperature difference (Figure 2e) caused by the shift of the GS temperature maximum (Figure 2d). Not all of the heat flux change is explained in this way. In particular, at other time scales, there is likely a role for other aforementioned processes also associated with the move to eddy-rich ocean (e.g., Fousard et al., 2018; Ma et al., 2015).

In Figure 2g and 2h, the different HH and HM distributions of precipitation, 925 hPa temperature gradientn and the surface storm track across the GS at 37ºN are examined. Relative to HM, the HH precipitation is suppressed over the lower temperature waters adjacent to the coast and increases abruptly to a maximum at the GS temperature maximum at 65ºW. In the vicinity of its GS (74ºW) HM greatly overestimates

Figure 1. HH control run mean minus HM control run mean for DJF: (a) SST (°C), (b) magnitude of the 925 hPa temperature gradient (°C m^{-1}), (c) sensible heat flux (W m^{-2}), (d) latent heat flux (W m^{-2}), (e) total precipitation rate (m s^{-1}), (f) convective precipitation rate (m s^{-1}), and (g) surface storm track (m s^{-1}). Thin black lines indicate 95% significance in the difference. Positive heat flux denotes more heat transfer from the ocean to the atmosphere. The yellow and gray lines near the US coast in panel (a) denote the different GS paths near Cape Hatteras for HM and HH, respectively. The GS path is defined by the location of the maximum SST at that latitude. The corresponding figures for the HH control run and the HM control run are shown in the supporting information.

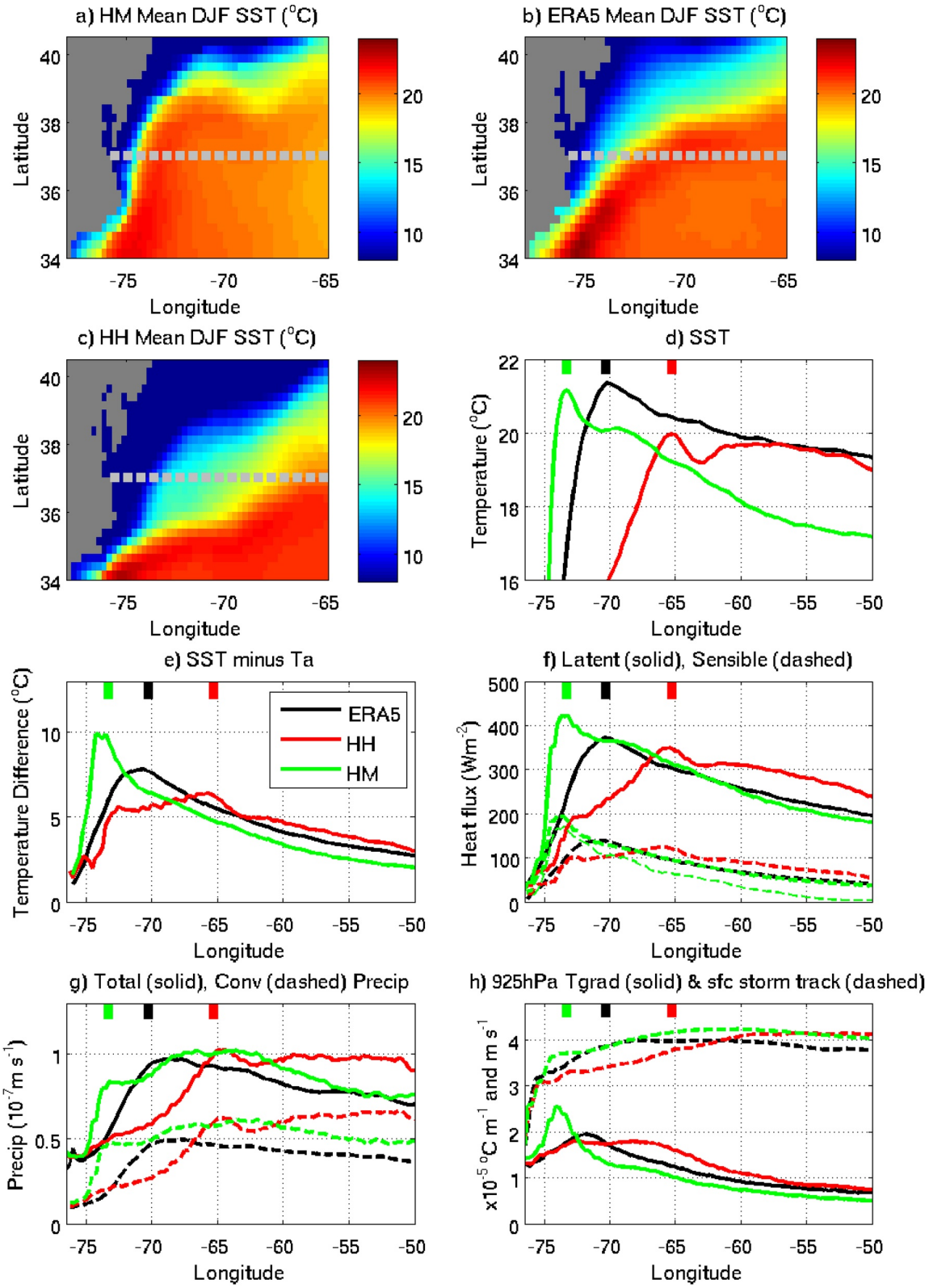
a) HM Mean DJF SST (°C)
b) ERA5 Mean DJF SST (°C)
c) HH Mean DJF SST (°C)
d) SST
e) SST minus Ta
f) Latent (solid), Sensible (dashed)
g) Total (solid), Conv (dashed) Precip
h) 925hPa Tgrad (solid) & sfc storm track (dashed)
Latitude
Longitude
Temperature (°C)
Temperature Difference (°C)
Heat flux (W/m-2)
Precip (10-7 m s-1)
x10-5 °C m-1 and m s-1
ERA5
HH
HM

precipitation, while HH underestimates by a similar magnitude at 70ºW (the location of the ERA GS). In general, we note the most marked difference in precipitation is associated with a change in the location of the maximum as opposed to a change in magnitude. This is contrast to Parfitt et al. (2017) who found a 30% increase in reanalysis precipitation associated with increased SST resolution. However this precipitation increase was attributed to increased gradients of SST and sensible heat which are not evident in the winter mean HH GS (Figures 2d and 2f). This does not eliminate the potential importance of this mechanism at the other time scales, such as that of individual storms (Vannière et al., 2017).

It is clear from Figure 2g that nearly all of the spatial differences in precipitation between HH and HM are convective in nature, highlighting the importance of the changes in air-sea exchanges just described. It is noted that the HH shift in convective precipitation maxima coincide spatially with the shifts in GS SST and turbulent flux maxima, but not the maximum SST gradient (which is slightly offset). However, this does not mean the SST gradient is not important in anchoring rainfall to the GS (Minobe et al., 2008). With regard to the lower tropospheric temperature gradient and the surface storm track, like the GS location itself, the locations of their maxima are over-corrected in HH. Coastward of its GS the surface storm track is too weak in HH. However, it is also clear that the magnitude of the near-shore (75ºW –70ºW) variation of the lower tropospheric temperature gradient is much improved in HH. In particular, while the magnitude of the HH maximum gradient is within 10% of ERA5, in HM there is a positive bias of over 30%.

In general, Figure 2 demonstrates the GS shift between HM and HH affects air-sea exchange and the overlying atmosphere. Although the HH GS is further away from ERA5 than HM at 37ºN, the bias in maximum air-sea temperature difference, turbulent fluxes and low-level temperature gradient is reduced when moving to the eddy-rich ocean. With regard to ERA5, we note that in common with all reanalyses the characteristics of the source data vary temporally, and in particular, the resolution of the source data, changes in 2007 (Hersbach et al., 2020; Hirahara et al., 2016). Despite this, the temporal standard deviation of the aforementioned key characteristics in Figure 2 (0.8°C air-sea temperature difference, 40 W m^{-2} sensible heat flux, and 2.5×10^{-6}°C m^{-1} 925 hPa temperature gradient) are smaller than the HH-HM differences.

In Figure 3a, we show the long term evolution of the distance of the GS separation from the coast at 37ºN for the two control simulations. Throughout the HH (HM) control run the GS separation remains hundreds of kilometers too far from (close to) the coast. The future projections will be discussed in the next section, but here in the context of Figure 3a we note the different future projected behavior of the HH GS. Whereas in HM the GS separation remains constant, in HH it slowly decreases to less than 50% of its original value.

3.3. Difference in Future Projections

Future projections of North Atlantic SSTs show two notable differences, both of which have a potential influence on mid-Atlantic storm tracks. First, for both simulations we note that the (anthropogenic) global warming signal, denoted by increases in the North Atlantic SSTs, is interrupted by a subpolar gyre warming hole (Drijfhout et al., 2012; Menary & Wood, 2018) (Figures 4a–4c). This is consistent with the marked decline in the AMOC in these simulations reported by Roberts et al. (2020). Recent work suggests a stronger AMOC decline in higher resolution models is related to a more saline mean state of the subpolar gyre (Jackson et al., 2020). As a consequence, the warming hole in HH is more pronounced, and represents actual cooling, up to 2°C, in some areas. It is anticipated that this could strengthen the temperature gradient of the overlying atmosphere on the southern and eastern flank of the warming hole.

The second noticeable difference in the SST projections is an enhanced warming in the GS region in HH, which is a manifestation of the aforementioned decrease in GS separation (Figure 3a). It has been argued

Figure 2. Location of Gulf Stream separation: mean DJF SST (°C) in GS region for (a) HM Control, (b) ERA5, (c) HH Control. (d) Mean DJF SST (°C) along 37ºN through the GS. Same as (d) but for (e) SST minus 2 m air temperature difference (°C), (f) surface latent, (solid lines) and sensible (dashed lines) heat flux (W m^{-2}), (g) total (solid lines) and convective precipitation (dashed lines) (10^{-7} m s^{-1}) and (h) 925 hPa temperature gradient (solid lines, 10^{-5}°C $^{-1}$ m^{-1}) and surface storm track (dashed lines, m s^{-1}). In (d), through (h) black lines denotes ERA5, green line HM control, red line HH control and the color-coded vertical bars denote the location of the GS (defined by the temperature maxima) in each of the simulations. In (f) the thin dashed green line is the estimate of HM by scaling HH by the ratio of HM:HH air-sea temperature differences (This quantifies the extent that differences air-sea temperature difference explains the difference in sensible heat flux between HH and HM). For means of comparison, the fields in (a and c) have been put on the same ERA5 grid and as ERA5 is not for 100 years all the means are for a 40-year period (ERA5 period used is 1979–80 to 2018–19).

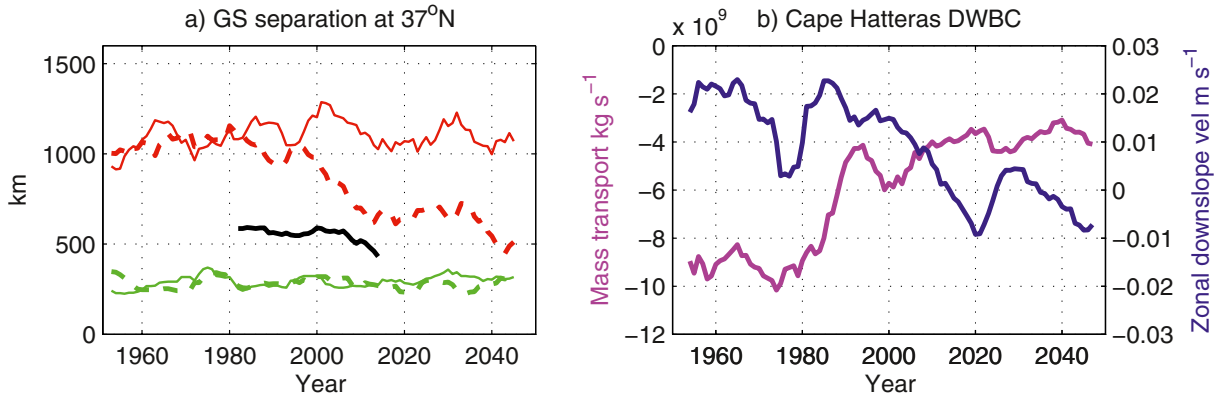

Figure 3. (a) Long-term evolution of the GS separation (km), measured by the distance of the maximum SST from the US coast at 37ºN (gray-dashed line in Figures 2a–2c). The black line denotes ERA5, the green line HM, the red line HH, solid lines are the control simulations and dashed lines the historical/future projection. (b) long-term evolution of the strength of the DWBC (magenta line) and near bottom zonal downslope flow at Cape Hatteras (blue line). In both (a and b) a 7-years running mean has been applied. DWBC transport is defined as the total southward only flow at Cape Hatteras (35ºN, below 200 m, west of 74.6ºW). Near bottom downslope flow is defined as the average velocity between 34ºN and 35ºN, 74ºW and 73ºW below 3,140 m (see Figure S4).

that strong warming of the north-west Atlantic is associated with a GS shift in response to Global Warming, but one which is only found in higher resolution eddy-rich simulations (Saba et al., 2016), despite observational evidence of enhanced warming in the region (Pershing et al., 2015). The argument proposes that a global warming induced AMOC decline results in a reduction in the strength of the deep western

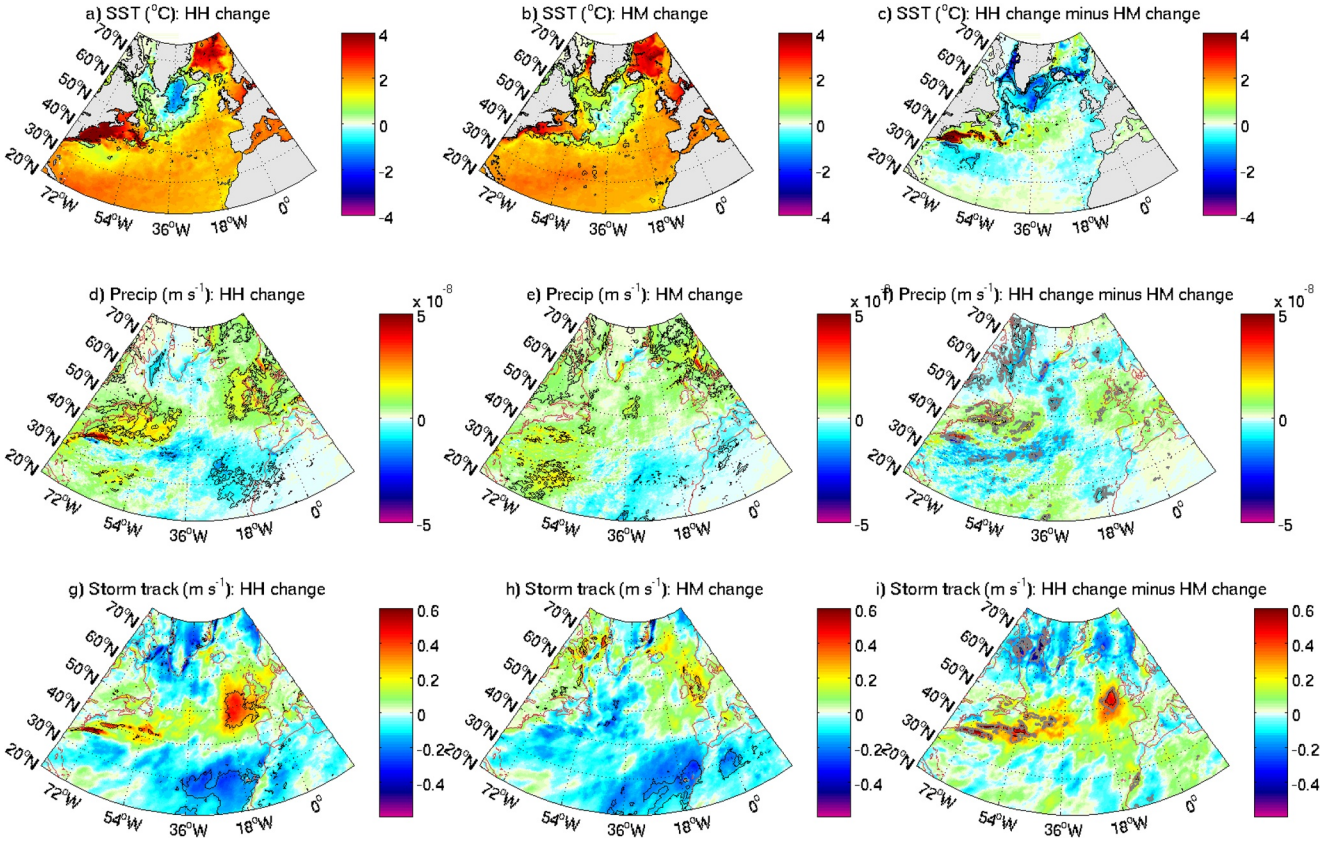

Figure 4. 2031–2050 minus 1951–1970 difference in: SST (°C) (a) HH and (b) HM); precipitation (m s^{-1}) (d) HH and (e) HM); storm track (m s^{-1}) (g) HH and (h) HM. Panels (c, f, and i) show the difference between the HH future change and the HM change. The black lines denote the 95% significance. On panels (c, f, and i) the 90% significance is also included (gray lines).

boundary current (DWBC). As the strength of the DWBC reduces so does the strength of the perpendicular (downslope) flow away from the DWBC. This means that downward bottom velocity is also reduced. Zhang and Vallis (2007) describe how the role of the bottom velocity is to promote positive vorticity and thus the GS separation at Cape Hatteras. The analysis here of HH confirms a projected decline in the DWBC (Figure 3b) and also the near bottom zonal velocity away from the DWBC (see also Figure S4). With regard to the near bottom velocity, we are not able to rule out the possibility that this is a response to, rather than a cause of a decreasing GS separation. However, the results are consistent with the contention that the decrease in GS separation is a response to a Global Warming induced AMOC decline found in eddy-rich simulations.

In terms of the future projections of precipitation, while HM produces a climate change signal of increased precipitation over the mid-latitude storm tracks (Figure 4e), consistent with many previous studies (e.g., Catto et al., 2019), this signal is stronger in HH (Figure 4d). In particular, HH significantly enhances the increased precipitation over the GS region and the eastern mid-latitude Atlantic (Figure 4f). In the latter region (20ºW to 0ºE, 50ºN to 60ºN), which encompasses the UK and Ireland, the precipitation increase doubles from 0.5×10^{-8} m s^{-1} in HM to 1.0×10^{-8} m s^{-1} (or 13 mm per month to 26 mm per month). In the case of HH, the change represents a 20% increase over the length of the 100 years simulation. With regard to the surface storm track there is relatively weak climate change signal in HM, which includes a modest strengthening over the eastern Atlantic and the British Isles (Figure 4h). In contrast HH has significant increases in storminess (of up to 0.5 m s^{-1}) over the GS and the eastern Atlantic (Figure 4g). These differences in storm projections between HH and HM are significant (Figure 4i). Considering the full 1950–2050 time series of the eastern Atlantic (20ºW to 10ºW, 45ºN to 55ºN) surface storm track, the trend is 3.5×10^{-3} m s^{-1} per year (±standard error of 1.1×10^{-3}), six times as much as HM ($0.5 \pm 1.1 \times 10^{-3}$ m s^{-1} per year) for the same region. We also note that other measures of storminess, such as the band-passed covariances of meridional wind and temperature and variance of meridional wind, also show enhanced Atlantic storminess (Figure S5) in HH. Although, in the upper troposphere the increase in HH storminess is not significantly greater than for HM, it is at lower levels. In particular, the increase levels of HH storminess at 850 and 1,000 hPa (Figure S5c and S5f) exhibit some similar spatial features as the surface storminess in Figure 4i.

We now briefly consider some of the processes that may connect the differences in SST projections to changes in precipitation and storminess. The projections of the 925 hPa temperature gradient, which indicates regions of baroclinic instability and promotes mid-latitude storm growth, broadly show a weakening in the western North Atlantic and a strengthening in the eastern subpolar Gyre (Figures 5a and 5b). In the west, HH has less gradient weakening between 40ºN and 60ºN and more weakening south of 40ºN associated with a combination of the GS shift and the stronger warming hole. In the east, strengthening of the temperature gradient is stronger in HH (35ºW to 20ºW, 50ºN to 60ºN) because of the stronger warming hole (Figures 4a and 4b). These changes are consistent with a stronger meridional temperature gradient in HH promoting greater increases in downstream storminess in the eastern Atlantic (Figures 4i and S5).

In addition to the influence of increased baroclinicity, we note a correspondence between projected changes in the surface turbulent fluxes (Figures 4d–4i) and precipitation/storminess. The spatial correlation values between surface storm track (Figure 4g and 4h) and latent heat flux (Figures 5d and 5e) between 35ºN and 60ºN are 0.52 for HH and 0.40 for HM. These spatial correlations illustrate that regions of projected increased latent heat flux correspond well with increases in storminess. Similarly, the enhanced precipitation-storminess regions in HH (Figure 4f and 4i) are associated with enhanced latent heat flux to the atmosphere. Particularly over the western Atlantic GS region, this is consistent with the higher coastal SSTs after a GS shift, promoting turbulent fluxes and low-level atmospheric instability. In their comparison of eddy-rich and non-eddy-rich control simulations, Small et al. (2019) attributed greater importance to increases in absolute SST, turbulent fluxes, and propensity for low-level atmospheric instability as opposed to large scale changes in the meridional temperature gradient. Here we note that the move to eddy-rich simulations creates differences in the SST projections that could allow both mechanisms to contribute to the more pronounced increase in future east Atlantic storminess.

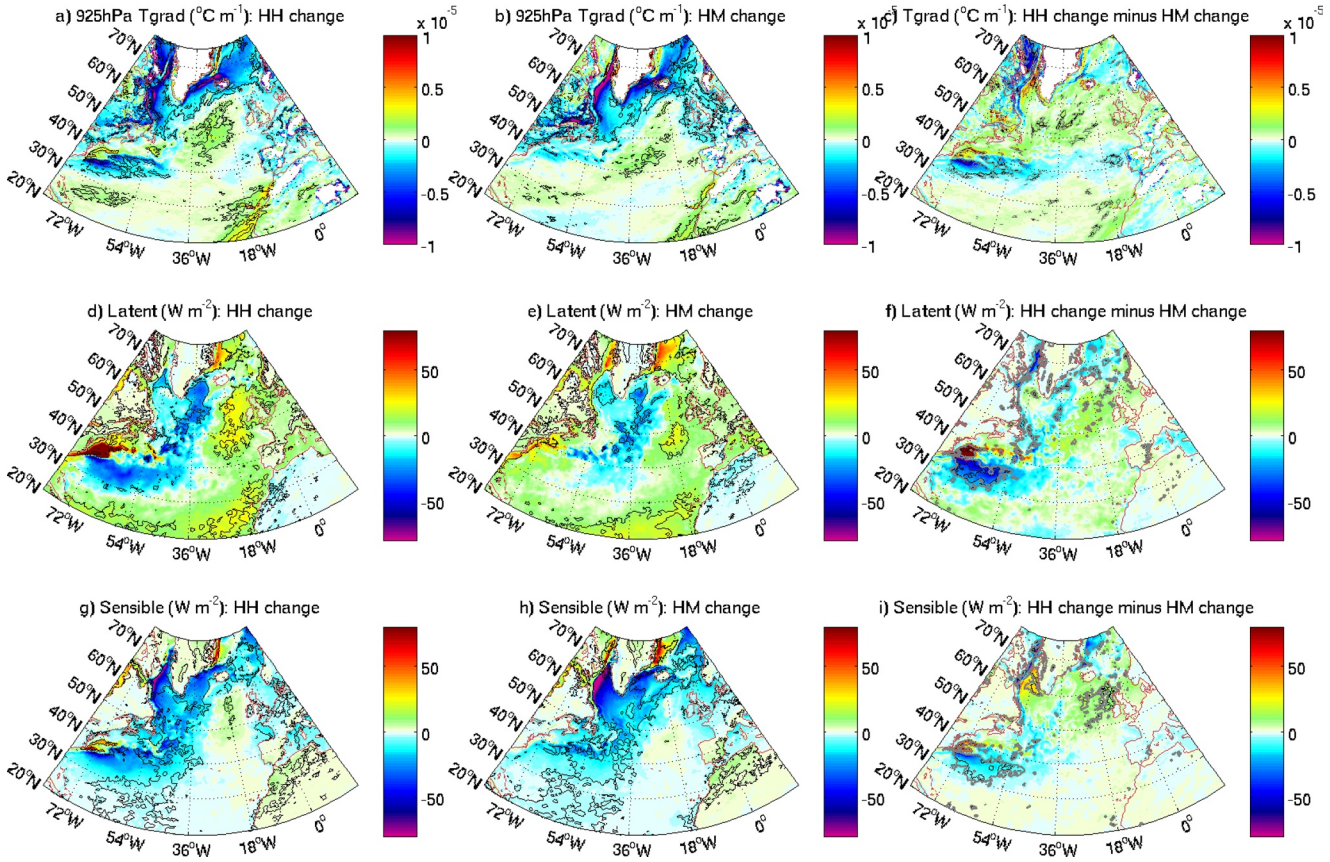

Figure 5. 2031–2050 minus 1951–1970 difference in; 925 hPa temperature gradient (°C m^{-1}) (a) HH and (b) HM); latent heat flux (W m^{-2}) (d) HH and (e) HM); sensible heat flux (W m^{-2}) (g and h). Panels (c, f, and i) show the difference between the HH future change and the HM change. The black lines denote the 95% significance. On panels (c, f, and i) the 90% significance is also included (gray lines).

4. Conclusions

This study has revealed significant changes in North Atlantic surface storm tracks and precipitation associated with the move to eddy-rich ocean resolution in climate models. In addition, we find that there is a larger projected change in the North Atlantic winter climate with an eddy-rich ocean. In particular, the future trend in east-Atlantic storminess is six times greater in the eddy-rich ocean climate model (HH) than in the eddy-permitting model (HM).

These changes are associated with two features of the SST field, namely (a) the strength of the subpolar gyre warming hole and (b) the temporal changes of the GS separation in the eddy-rich simulation. Understanding and assessing the authenticity of these new depictions of the future evolution of North Atlantic SSTs is critical in assessing the reliability of the latest projections of mid-latitude storms. Concerning the stronger warming hole, this is a response to a stronger AMOC decline in the eddy-rich simulations. While this stronger decline is found in some other eddy-rich simulations (Saba et al., 2016), the reason for it is still under investigation; in particular, it might reflect mean state bias in the eddy-rich model (Jackson et al., 2020).

With regard to the changes in the GS, there is a slightly mixed picture from recent high-resolution modeling results. Alexander et al. (2020) forced the eddy-rich Regional Ocean Modeling System with output from the RCP8.5 projections of three CMIP5 models. Although there was enhanced warming to the north-west of the GS (see Figure 3), the range of warming in the experiments was large, and the authors found they could not be attributed to changes in the GS location. However, coastal warming and shifts in the GS have been found in eddy-rich climate change simulations of coupled models such as GFDL CM2.6 (Saba et al., 2016) and the Community Earth System Model version 1 (R. J. Small, pers. commun., 2020). These results suggest

that the decrease in GS separation may be a robust feature of ocean eddy-rich simulations in fully coupled global climate models.

The decrease in the GS separation in the eddy-rich simulation documented here reflects a mechanism not present in the eddy-permitting simulation where the GS (incorrectly) does not separate at Cape Hatteras. Although it is too early to determine if this GS shift is an actual response to climate change, there is some evidence of the corresponding enhanced coastal warming in recent observations (e.g., Poppick, 2018; Wu et al., 2012). With regard to this particular eddy-rich simulation, it is noted that the GS is too far separated from the coast to start with, and thus its coastward migration is greater than can occur in the real world. The implication of this is that the effect on SST, surface fluxes, and storminess may also be over-estimated.

This analysis illustrates that increased ocean resolution can reduce important model biases, for example, the location of the GS separation and associated local maxima in air-sea temperature difference and lower tropospheric temperature gradient. The removal of such biases could potentially lead to a different future projection of ocean temperature (as in the case in the model we have analyzed), thus allowing processes to operate that reveal potential future climate risks such as mid-latitude storms. However, given the above discussion of the results, an ensemble of simulations may be required to assess the range of possible impacts on future projections of the North Atlantic climate that result from the move to eddy-rich oceans. We also note that a parallel consideration of the atmospheric resolution is also important. In a recent complementary study atmosphere resolution was increased from 135 to 25 km in the atmosphere only version of the model used here (Baker et al., 2019). It was found the 25 km resolution significantly enhanced the climate change signal of the North Atlantic storm track.

In summary, an analysis of a climate model with different ocean resolutions has shown a much greater increase in east Atlantic storminess in a future projection of an eddy-rich ocean simulation relative to the eddy-permitting simulation. This difference reflects the different evolution of North Atlantic Ocean circulation and SSTs in the model simulations.

Data Availability Statement

The ERA5 reanalysis data set is available from https://www.ecmwf.int/en/forecasts/datasets/reanalysis-datasets/era5. Some of the model runs used the ARCHER UK National Supercomputing Service (http://www.archer.ac.uk).

Acknowledgments
Model data used in the present analysis are available from the CMIP6 Earth System Grid Federation and can be located using the information in M. Roberts (2017a, 2017b) for resolutions HM and HH, respectively, and Coward and Roberts (2018) for HH. JG, SJ, and MR gratefully acknowledge the support of the project PRIMAVERA, Grant Agreement 641727 of the Horizon 2020 research program. In addition JG, SJ, BS, and JC acknowledge support from the UK Natural Environment Research Council program 'Emergence of Climate Hazards' Grant No. NE/J013137/1. SJ and BS also acknowledge support from the UK Natural Environment Research Council ACSIS program (Ref. No. NE/N018044/1). MR was supported by the Met Office Hadley Center Climate Program funded by BEIS and Defra (GA01101).

References

Alexander, M. A., Shin, S., Scott, J. D., Curchitser, E., & Stock, C. (2020). The response of the northwest Atlantic Ocean to climate change. *Journal of Climate*, *33*, 405–428. https://doi.org/10.1175/jcli-d-19-0117.1

Baker, A. J., Schiemann, R., Hodges, K. I., Demory, M.-E., Mizielinksi, M. S., Roberts, M. J., et al. (2019). Enhanced climate change response of wintertime North Atlantic circulation, cyclonic activity, and precipitation in a 25-km-resolution global atmospheric model. *Journal of Climate*, *32*, 7763–7781. https://doi.org/10.1175/JCLI-D-19-0054.1

Booth, J. F., Kwon, Y.-O., Ko, S., Small, R. J., Msadek, R. (2017). Spatial patterns and intensity of the surface storm tracks in CMIP5 models. *Journal of Climate*, *30*, 4965–4981. https://doi.org/10.1175/JCLI-D-16-0228.1

Booth, J. F., Thompson, L., Patoux, J., & Kelly, K. A. (2012). Sensitivity of midlatitude storm intensification to perturbations in the sea surface temperature near the Gulf Stream. *Monthly Weather Review*, *140*, 1241–1256. https://doi.org/10.1175/mwr-d-11-00195.1

Bryan, F. O., Hecht, M. W., & Smith, R. D. (2007). Resolution convergence and sensitivity studies with North Atlantic Circulation models. Part 1. The western boundary current system. *Ocean Modelling*, *16*, 141–159. https://doi.org/10.1016/j.ocemod.2006.08.005

Catto, J. L., Ackerley, D., Booth, J. F., Champion, A. J., Colle, B. A., Pfahl, S., et al. (2019). The future of midlatitude cyclones. *Current Climate Change Report*, *5*, 407–420. https://doi.org/10.1007/s40641-019-00149-4

Catto, J. L., Jakob, C., Berry, G., & Nicholls, N. (2012). Relating global precipitation to atmospheric fronts. *Geophysics Research Letters*, *39*, L10805. https://doi.org/10.1029/2012GL051736

Chang, P., Zhang, S., Danabasoglu, G., Yeager, S. G., Fu, H., Wang, H., et al. (2020). An unprecedented set of high-resolution earth system simulations for understanding multiscale interactions in climate variability and change. *Journal of Advances in Modeling Earth Systems*, *12*, e2020MS002298. https://doi.org/10.1029/2020ms002298

Chassignet, E. P., & Marshall, D. P. (2008). Gulf Stream separation in numerical ocean models. *AGU Geophysical Monograph Series*, *177*. https://doi.org/10.1029/177GM05

Collins, M., Knutti, R., Arblaster, J., Dufresne, J.-L., Fichefet, T., Friedlingstein, P., et al. (2013). Long-term climate change: Projections, commitments and irreversibility. In T. F. Stocker, et al., (Eds.), *Climate change 2013: The Physical Science Basis. Contribution of working Group I to the Fifth Assessment Report of the Intergovernmental panel on climate change*. Cambridge University Press.

Collins, M., Minobe, S., Barreiro, M., Boroni, S., Kaspi, Y., Kuwano-Yoshida, A., et al. (2018). Challenges and opportunities for improved understanding of regional climate dynamics. *Nature Climate Change*, *8*, 101–108. https://doi.org/10.1038/s41558-017-0059-8

Coward, A., & Roberts, M. (2018). *NERC HadGEM3-GC31-HH model output prepared for CMIP6 HighResMIP*. Earth System Grid Federation. https://doi.org/10.22033/ESGF/CMIP6.1822

Czaja, A., Frankignoul, C., Minobe, S., & Vannière, B. (2019). Simulating the midlatitude atmospheric circulation: What might we gain from high-resolution modeling of air–sea interactions? *Current Climate Change Reports*, *5*(4), 390–406. https://doi.org/10.1007/s40641-019-00148-5

de Vries, Scher, H. S., Haarsma, R., Drijfhout, S., & van Delden, A. (2019). How Gulf-Stream SST-fronts influence Atlantic winter storms. *Climate Dynamics*, *52*, 5899–5909. https://doi.org/10.1007/s00382-018-4486-7

Drijfhout, S., van Oldenborgh, G. J., & Cimatoribus, A. (2012). Is a decline of AMOC causing the warming hole above the North Atlantic in observed and modeled warming patterns? *Journal of Climate*, *25*, 8373–8379. https://doi.org/10.1175/jcli-d-12-00490.1

Foussard, A., Lapeyre, G., & Plougonven, R. (2019). Storm track response to ocean eddies in idealized atmospheric simulations. *Journal of Climate*, *32*, 445–463. https://doi.org/10.1175/JCLI-D-18-0415.1

Giordani, H., & Caniaux, G. (2001). Sensitivity of cyclogenesis to sea surface temperature in the Northwestern Atlantic. *Monthly Weather Review*, *129*, 1273–1295. https://doi.org/10.1175/1520-0493(2001)129<1273:soctss>2.0.co;2

Haarsma, R. J., & Coauthors (2016). High Resolution Model Intercomparison Project (HighResMIP v1.0) for CMIP6. *Geoscientific Model Development*, *9*, 4185–4208. https://doi.org/10.5194/gmd-9-4185-2016

Hersbach, H., Bell, B., Berrisford, P., Hirahara, S., Horányi, A., Muñoz-Sabater, J., et al. (2020). The ERA5 global reanalysis. *Quarterly Journal of Royal Meteorological Society*, *146*, 1999–2049. https://doi.org/10.1002/qj.3803

Hirahara, S., Balmaseda, M. A., de Boisseson, E., & Hersbach, H. (2016). *Sea surface temperature and sea ice concentration for ERA5. ERA Report series 26. 25pp*. European Centre for Medium Range Weather Forecasts. https://www.ecmwf.int/file/46880/download?token=4pKnkudy

Jackson, L. C., Roberts, M. J., Hewitt, H. T., Iovino, D., Koenigk, T., Meccia, V. L., et al. (2020). Impact of ocean resolution and mean state on the rate of AMOC weakening. *Climate Dynamics*, *55*, 1711–1732. https://doi.org/10.1007/s00382-020-05435-9

Joyce, T., Kwon, Y. O., & Yu, L. (2009). On the relationship between synoptic wintertime atmospheric variability and path shifts in the Gulf Stream and the Kuroshio Extension. *Journal of Climate*, *22*, 3177–3192. https://doi.org/10.1175/2008jcli2690.1

Kuo, Y.-H., Reed, R. J., & Low-Nam, S. (1991). Effects of surface energy fluxes during the early development and rapid intensification stages of seven explosive cyclones in the western Atlantic. *Monthly Weather Review*, *119*, 457–475. https://doi.org/10.1175/1520-0493(1991)119<0457:eosefd>2.0.co;2

Lee, R. W., Woollings, T. J., Hoskins, B. J., Williams, K. D., O'Reilly, C. H., & Masato, G. (2018). Impact of Gulf Stream SST biases on the global atmospheric circulation. *Climate Dynamics*, *51*, 3369–3387. https://doi.org/10.1007/s00382-018-4083-9

Ma, X., Chang, P., Saravanan, R., Montuoro, R., Hsieh, J.-S., Wu, D., et al. (2015). Distant influence of Kuroshio Eddies on North Pacific Weather Patterns? *Scientific Reports*, *5*, 17785. https://doi.org/10.1038/srep17785

Ma, X., Jing, Z., Chang, P., Liu, X., Montuoro, R., Small, R. J., et al. (2016). Western boundary currents regulated by interaction between ocean eddies and the atmosphere. *Nature*, *535*(7613), 533–537. https://doi.org/10.1038/nature18640

Marzocchi, A., Hirschi, J. J.-M., Holliday, N. P., Cunningham, S. A., Blaker, A. T., & Coward, A. C. (2015). The North Atlantic subpolar circulation in an eddy-resolving global ocean model. *Journal of Marine System*, *142*, 126–143. https://doi.org/10.1016/j.marsys-.2014.10.00710.1016/j.jmarsys.2014.10.007

Menary, M. B., & Wood, R. A. (2018). An anatomy of the projected North Atlantic warming hole in CMIP5 models. *Climate Dynamics*, *50*, 3063–3080. https://doi.org/10.1007/s00382-017-3793-8

Minobe, S., Kuwano-Yoshida, A., Komori, N., Xie, S.-P., & Small, R. J. (2008). Influence of the Gulf Stream on the troposphere. *Nature*, *452*, 206–210. https://doi.org/10.1038/nature06690

Nakamura, M., Sampe, T., Tanimoto, Y., & Shimpo, A. (2004). Observed associations among storm tracks jet streams and midlatitude oceanic fronts. *AGU Geophysics Monograph Series*, *147*, 329–345. https://doi.org/10.1029/147GM18

Parfitt, R., Czaja, A., Kwon, Y. O. (2017). The impact of SST resolution change in the ERA-Interim reanalysis on wintertime Gulf Stream frontal air-sea interaction. *Geophysical Research Letters 44*(7), 3246–3254.

Parfitt, R., Czaja, A., Minobe, S., & Kuwano-Yoshida, A. (2016). The atmospheric frontal response to SST perturbations in the Gulf Stream region. *Geophysical Research Letters*, *43*, 2299–2306. https://doi.org/10.1002/2016GL067723

Parfitt, R., & Kwon, Y. O. (2020). The modulation of Gulf Stream influence on the troposphere by the eddy-driven jet. *Journal of Climate*, *33*, 4109–4120. https://doi.org/10.1175/jcli-d-19-0294.1

Pershing, A. J., Alexander, M. A., Hernandez, C. M., Kerr, L. A., Le Bris, A., Mills, K. E. (2015). Slow adaption in the face of rapid warming leads to collapse of the Gulf of Maine cod fishery. *Science*, *350*, 809–812. https://doi.org/10.1126/science.aac9819

Poppick, L. (2018). Why is the Gulf of Maine warming faster than 99% of the ocean? *EOS*, *99*. https://doi.org/10.1029/2018EO109467

Priestley, M. D. K., Ackerley, D., Catto, J. L., Hodges, K. I., McDonald, R. E., & Lee, R. W. (2020). An overview of the Extratropical Storm Tracks in CMIP6 historical simulations. *Journal of Climate*, *33*(15), 6315–6343. https://doi.org/10.1175/JCLI-D-19-0928.1

Renault, L., Molemaker, M. J., Gula, J., Masson, S., & McWilliams, J. C. (2016). Control and stabilization of the Gulf Stream by oceanic current interaction with the atmosphere. *Journal of Physical Oceanography*, *46*(11), 3439–3453. https://doi.org/10.1175/jpo-d-16-0115.1

Riahi, K., van Vuuren, D. P., Kriegler, E., Edmonds, J., O'Neill, B. C., Fujimori, S., et al. (2017). The shared socioeconomic pathways and their energy, land use, and greenhouse gas emissions implications: An overview. *Global Environmental Changes*, *42*, 153–168. https://doi.org/10.1016/j.gloenvcha.2016.05.009

Roberts, M. (2017a). *MOHC HadGEM3-GC31-HM model output prepared for CMIP6 HighResMIP*. Earth System Grid Federation. https://doi.org/10.22033/ESGF/CMIP6.446

Roberts, M. (2017b). *MOHC HadGEM3-GC31-HH model output prepared for CMIP6 HighResMIP*. Earth System Grid Federation. http://cera-www.dkrz.de/WDCC/meta/CMIP6/CMIP6.HighResMIP.MOHC.HadGEM3-GC31-HH.Refstyled

Roberts, M. J., Baker, A., Blockley, E. W., Calvert, A., Hewitt, H. T., Jackson, L.C., et al. (2019). Description of the resolution hierarchy of the global coupled HadGEM3-GC3.1 model as used in CMIP6 HighResMIP experiments. *Geoscientific Model Development*, *12*, 4999–5028. https://doi.org/10.5194/gmd-12-4999-2019

Roberts, M. J., Jackson, L. C., Roberts, C. D., Meccia, V., Docquier, D., Koenigk, T., et al. (2020). Sensitivity of the Atlantic meridional overturning circulation to model resolution in CMIP6 HighResMIP simulations and implications for future changes. *Journal of Advances in Modeling Earth Systems*, *12*, e2019MS002014. https://doi.org/10.1029/2019MS002014

Saba, V. S., Griffies, S. M., Anderson, W. G., Winton, M., Alexander, M. A., Delworth, T. L., et al. (2016). Enhanced warming of the Northwest Atlantic Ocean under climate change. *Journal of Geophysical Research: Oceans*, *121*, 118–132. https://doi.org/10.1002/2015JC011346

Schoonover, J., Dewar, W. K., Wienders, N., & Deremble, B. (2017). Local sensitivities of the Gulf Stream separation. *Journal of Physical Oceanography*, *47*(2), 353–373. https://doi.org/10.1175/jpo-d-16-0195.1

Sheldon, L., Czaja, A., Venoit, B., Morcrette, C., Sohet, B., Casado, M., & Smith, D. (2017). A 'warm path' for Gulf Stream-troposphere interactions. *Tellus*, *69*, 1299397. https://doi.org/10.1080/16000870.2017.1299397

Siqueira, L., Kirtman, B. P., & Laurindo, L. C. (2021). Forecasting remote atmopsheric responses to decadal Kuroshio stability transitions. *Journal of Climate*, *34*, 379–395. https://doi.org/10.1175/jcli-d-20-0139.1

Small, R. J., Msadek, R., Kwon, Y.-O., Booth, J. F., & Zarzycki, C. (2019). Atmosphere surface storm track response to resolved ocean mesoscale in two sets of global climate model experiments. *Climate Dynamics*, *52*, 2067–2089. https://doi.org/10.1007/s00382-018-4237-9

Smirnov, D., Newman, M., Alexander, M. A., Kwon, Y. O., & Frankignoul, C. (2015). Investigating the local atmospheric response to a realistic shift in the Oyashio sea surface temperature front. *Journal of Climate*, *28*, 1126–1147. https://doi.org/10.1175/jcli-d-14-00285.1

Vannière, B., Czaja, A., Dacre, H., & Woollings, T. (2017). A 'cold path' for the Gulf Stream-troposphere connection. *Journal of Climate*, *30*, 1363–1379. https://doi.org/10.1175/jcli-d-15-0749.1

Williams, K. D., Copsey, D., Blockley, E. W., Bodas-Salcedo, A., Comer, C. R., Davis, P., et al. (2017). The Met Office Global Coupled Model 3.0 and 3.1 (GC3.0 and GC3.1) Configurations. *Journal of Advances in Modeling Earth Systems*, *10*, 357–380. https://doi.org/10.1002/2017MS001115

Woollings, T., Gregory, J. M., Pinto, J. G. M., & Brayshaw, D. J. (2012). Response of the North Atlantic storm track to climate change shaped by ocean–atmosphere coupling. *Nature Geoscience*, *5*, 313–317. https://doi.org/10.1038/ngeo1438

Wu, L., Cai, W., Zhang, L., Nakamura, H., Timmermann, A., Joyce, T., et al. (2012). Enhanced warming over the global subtropical western boundary currents. *Nature Climate Change*, *2*(3), 161–166. https://doi.org/10.1038/nclimate1353

Zappa, G., Shaffrey, L. C., Hodges, K. I. P. G. S., & Stephenson, D. B. (2013). A multimodel assessment of future projections of North Atlantic and European extratropical cyclones in the CMIP5 climate models. *Journal of Climate*, *26*, 5846–5862. https://doi.org/10.1175/JCLI-D-12-00573.1

Zhang, R., & Vallis, G. K. (2007). The role of bottom vortex stretching on the path of the North Atlantic Western Boundary Current and on the Northern Recirculation Gyre. *Journal of Physical Oceanography*, *37*, 2053–2080. https://doi.org/10.1175/jpo3102.1

Zwiers, F. W., & Von Storch, H. (1995). Taking serial correlation into account in tests of the mean. *Journal of Climate*, *8*, 336–351. https://doi.org/10.1175/1520-0442(1995)008<0336:tsciai>2.0.co;2